Int. J. Electron. Commun. (AEÜ) 128 (2021) 153519

Contents lists available at ScienceDirect

Int. J. Electron. Commun. (AEÜ)

journal homepage: www.elsevier.com/locate/aeue

Regular paper

Field Asymmetry Ratio: A new quantitative parameter to select microstrip antenna geometries for low cross-polarization application

Susamay Samanta [a,*], P Soni Reddy [b], Kaushik Mandal [c]

[a] Department of Electronics & Communication Engineering, School of Engineering and Technology, Adamas University, Kolkata 700126, India
[b] Department of Engineering & Technological Studies, University of Kalyani, West Bengal 741235, India
[c] Institute of Radio Physics and Electronics, University of Calcutta, Kolkata 700009, India

ARTICLE INFO

Keywords:
Cross-polarization suppression
Point-symmetric geometry
Field Asymmetry Ratio
Microstrip patch antenna
Shorting pins

ABSTRACT

This paper proposes a new quantitative parameter on identifying the primary factor for appropriate geometry selection of microstrip patch antennas dedicated to low cross-polarization (XP) applications. The significance of point-symmetric (PS) and non-point-symmetric (NPS) geometries has been analyzed on the basis of 'Field Asymmetry Ratio' (FAR), a new parameter, defined to quantify the level of electric field asymmetry leading to XP radiation in any regular shaped microstrip patch antennas. Based on this analysis, a conclusive inference has been established on the importance of point-symmetric patch geometry selections to achieve lower XP radiation. The 6-element circular cluster of shorting pins (CCSP) has been adopted as the XP suppression tool for S-band applications to validate the proposition. An XP suppression of approximately 9 dB at the boresight and 5 dB at ±30° around the boresight in H-plane has been achieved for the square-shaped patch geometry.

1. Introduction

Cross-polarization discrimination (XPD) in microstrip patch antennas (MSA) is an important aspect for meeting the diverse needs of high accuracy positioning systems [1] as per the European Telecommunications Standards Institute (ETSI) standard [2].

In case of tracking and surveillance radar, arbitrarily polarized signal components scattered from a radar target can make boresight location appear to shift at irregular time intervals [3]. This boresight uncertainty or boresight jitter can enforce significant restrictions upon radar tracking accuracy levels by means of false target detection. Therefore, a high XP isolation at the boresight and throughout the half-power beamwidth should be the prime focus to design such antennas.

Usually, regular patch geometries can be broadly classified as point-symmetric (PS) and non-point-symmetric (NPS). Among PS geometries, rectangle and circle were the foremost patch geometries that were investigated for XP analysis [4–16]. XP characterization of PS patch geometries based on antenna design parameters has been presented in [4–6]. Oberhart et al. [4] analyzed the rectangular patch and established a correlation between the XP levels with the patch aspect ratio. Huynh et al. [5] presented a more detailed study in this regard and established other antenna design factors like — feed position, substrate thickness, substrate permittivity, and resonance frequency for controlling the patch XP levels. Lee et al. [6] performed a similar analysis for the circular patch and validated the findings made in [4] and [5].

XP characterization of PS patch geometries using modal analysis has been presented in [7,8,10,12,13]. Guha et al. in their research works [7,8] introduced modal analysis for patch XP characterization by identifying the first higher mode as a key factor towards increased XP levels in circular, square, and rectangular patch geometries. Samanta et al. presented similar modal analysis for XP characterization of hexagonal [10], circular [12], and diamond-shaped [13] patch geometries. Few studies on XP characterization using near-field analysis for rectangular [9] and circular [14] patch geometries were also conducted. Recently, studies on the XP characterization of PS patch geometries using surface current distribution on the ground plane [11]/patch [15]/feed [16] has been conducted. In almost all of the research works documented so far on XP suppression, the importance of point symmetry in patch geometry was not analyzed explicitly and the XP characterization of different NPS geometries has remained unattended. Coincidentally, the patch geometries explored till date in this domain are all PS. However, the basic reason behind choosing the PS geometries for XP suppression works remains unexplored.

In this paper, the inherent geometrical implication of a patch on XP radiation is examined for the first time. This work focuses on establishing a quantitative measure of E-field asymmetry on the patch and its significance in XP characterization of microstrip patch antennas of different geometry. Commonly used microstrip antenna patch geometries: triangle (TMSA) and square (SMSA) have been considered

* Corresponding author.
E-mail address: samantasusamay@gmail.com (S. Samanta).

https://doi.org/10.1016/j.aeue.2020.153519
Received 4 June 2020; Accepted 21 October 2020
Available online 27 October 2020

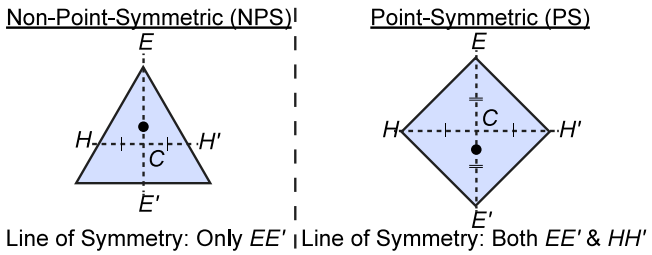

Fig. 1. Visualization of the structural symmetry in PS and NPS patch geometries. EE': E-plane and HH': H-plane. C is the center of the geometry and the black dot represents the feed location.

to identify the role played by the 'point symmetry' in their XP characterization. Subsequently, the higher level of XP radiation in NPS geometry compared to the PS geometry has been revealed based on the proposed field asymmetry ratio (FAR) parameter. Circular clusters of shorting pins (CCSP), one of the recent XP suppression tools introduced in [12], has further been used to validate the concept of FAR for the PS patch geometry. The proposed study aims to open up new scopes to explain the XP performance of microstrip patch antennas having any arbitrary patch shape and help an antenna designer to choose the right geometry for low XP applications. Ansys® HFSS™ software was used for simulation of all antenna configurations.

2. Interdependency of patch geometrical symmetry and XP

2.1. Concept of point symmetry

Any regular patch geometry is said to be PS if there exists a central point (C) such that every point lying on the patch geometry has another point equidistant from the center and directly opposite to it as shown in Fig. 1. Regular patch geometries having even numbers of sides like square are thus PS while the ones having the odd number of sides like triangle are NPS geometries.

2.2. Role of 'Geometrical Asymmetry' behind XP generation for different regular patch geometries

NPS (TMSA) and PS (SMSA) microstrip antennas are designed for the S-band using low loss fiberglass-PTFE woven composite material (Rogers DiClad® 870) of dielectric constant (ϵ_r) 2.33, height (h) 1.575 mm and loss tangent ($\tan\delta$) 0.0013. The patch geometries have been designed with an area equal to that of the circular MSA resonating at 3.6 GHz [17] for analytical simplicity. Coaxial probe feed at optimally matched position is used for feeding all the patch designs.

As shown in Fig. 1, the PS patch geometry (SMSA) is found to possess structural symmetry across both E and H-plane. On the contrary, NPS geometry (TMSA) although having structural symmetry across the E-plane, possesses inherent asymmetry across the H-plane. The dominant mode E-field distribution for both the patch geometries under consideration is shown in Fig. 2. Considering the E-plane (EE'), in both the patch geometries the average E-field strength on either side of E-plane, i.e. E_{1E} and E_{2E} are nearly equal due to the structural symmetry possessed by both the NPS and PS geometries across the E-plane. Considering the H-plane (HH'), a clear asymmetry in dominant mode E-field distribution across the H-plane is observed for both the patch geometries. This asymmetry is significantly higher in the NPS geometry compared to the PS geometry. In case of PS geometry (SMSA) significant E-field asymmetry is visible on either side of the H-plane, i.e. $E_{1H} \neq E_{2H}$ despite the structural symmetry across the H-plane. Also, the average E-field strength on the patch half containing the feed is greater compared to the other half, i.e. $E_{1H} > E_{2H}$. Thus, the E-field asymmetry on either side of the H-plane for PS geometry is solely due to the offset positioning of the coaxial probe (i.e. probe position asymmetry). In case of NPS geometry (TMSA), the average E-field strength on either side of the H-plane is found to be imbalanced, i.e. $E_{1H} \neq E_{2H}$ and $E_{1H} > E_{2H}$. This field asymmetry across the H-plane is mainly observed due to two factors — inherent structural asymmetry in the NPS geometries and probe position asymmetry.

Thus, based on the above observation an attempt has been made to analyze the degree of asymmetry in E-field strength for both the patch geometries quantitatively. In this context, a new quantitative parameter, Field-Asymmetry Ratio (FAR), is introduced for the numerical representation of this field asymmetry on either side of the E and H-plane. $FAR_{E-plane}$ is the numerical representation of field asymmetry on either side of the E-plane. $FAR_{E-plane}$ for any patch geometry is defined as follows.

$$FAR_{E-plane} = \frac{E_{1E}}{E_{2E}} - 1 \tag{1}$$

where, E_{1E} and E_{2E} are the respective average E-field strength values on either side of the patch geometry considering the vertical line-of-reference (E-plane, EE') as shown in Fig. 2. Subscript '1' is used to represent higher values and the subscript '2' is used to represent lower value of the average E-field strength, irrespective of the side of the patch geometry. The dominant mode E-field distribution for conventional patch geometries (PS/NPS) given in Fig. 2 shows that with respect to EE', $E_{1E} \neq E_{2E}$ and $E_{1E} > E_{2E}$. Similarly, $FAR_{H-plane}$ is the numerical representation of field asymmetry on either side of the H-plane. $FAR_{H-plane}$ is defined for any patch geometries considering the horizontal line-of-reference (H-plane, HH') as given below.

$$FAR_{H-plane} = \frac{E_{1H}}{E_{2H}} - 1 \tag{2}$$

where, E_{1H} and E_{2H} are the respective average E-field strength values on either side of the patch geometry considering the horizontal line-of-reference (H-plane, HH') as shown in Fig. 2. Subscript '1' is used to represent higher values and the subscript '2' is used to represent lower value of the average E-field strength, irrespective of the side of the patch geometry. The dominant mode E-field distribution for conventional patch geometries (PS/NPS) given in Fig. 2 shows that with respect to HH', $E_{1H} \neq E_{2H}$. The average E-field strength value on the patch half containing the feed is greater compared to that on the other half. Therefore, average E-field strength value on the patch half containing the feed is denoted as E_{1H} and the average E-field strength value on the other half of the patch is denoted as E_{2H}. Thus, $E_{1H} > E_{2H}$. The flowchart enlisting the steps for calculating FAR in detail for any patch geometry (PS/NPS) is shown in Fig. 3.

Ideally, according to the traditional cavity model for probe-fed microstrip antennas [9], considering pure dominant mode resonance, the E-fields on either side of the E-plane and H-plane should be symmetric. Thus, the $FAR_{E-plane}$ and $FAR_{H-plane}$ should ideally be zero. But practically due to geometrical asymmetry and probe offset positioning non-zero values of $FAR_{E-plane}$ and $FAR_{H-plane}$ are observed. Table 1 summarizes the FAR values for both the conventional patch geometries under test. The feed position and corresponding impedance values for each geometry are also provided in Table 1 for reference.

A near-to-ideal field symmetry of both PS (SMSA) and NPS (TMSA) geometries is observed across the E-plane (≈ 5%–6% deviation only). But a significantly high field asymmetry (≈ 20% for SMSA and 29% for TMSA) is visible across the H-plane. Compared to PS geometry, NPS geometry display greater field asymmetry across the H-plane.

Further, the XPD values at $\theta = 0°$(i.e. XPD at boresight or BXPD) for both the regular patch geometries under test are calculated from their simulated far-field characteristics in the H-plane as shown in Fig. 4 and are given in Table 1. Compared to NPS (TMSA), PS (SMSA) geometry provides a 7 dB higher XPD at boresight. For the MSAs, the XP in E-plane is inherently low as predicted by the cavity model [18], hence the main focus of this study is only on the H-plane XP pattern.

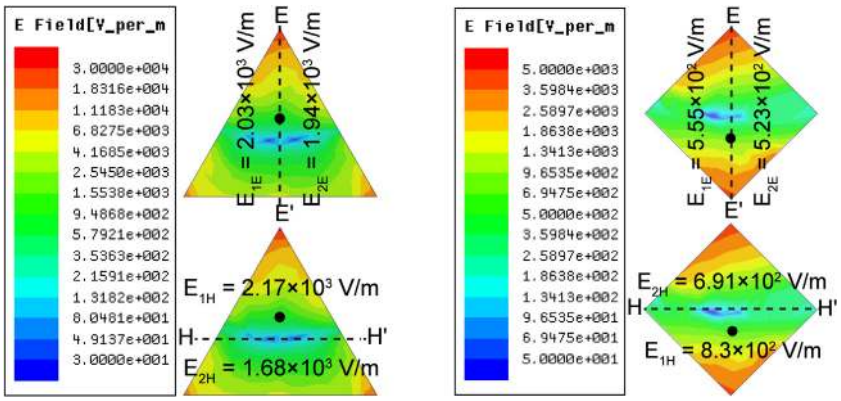

(a) Triangular Patch (TMSA) (b) Square Patch (SMSA)

Fig. 2. Dominant mode E-field distribution for conventional TMSA and SMSA. Black dot represents the feed location. All values indicated on the patch are the respective average E-field strengths in that region.

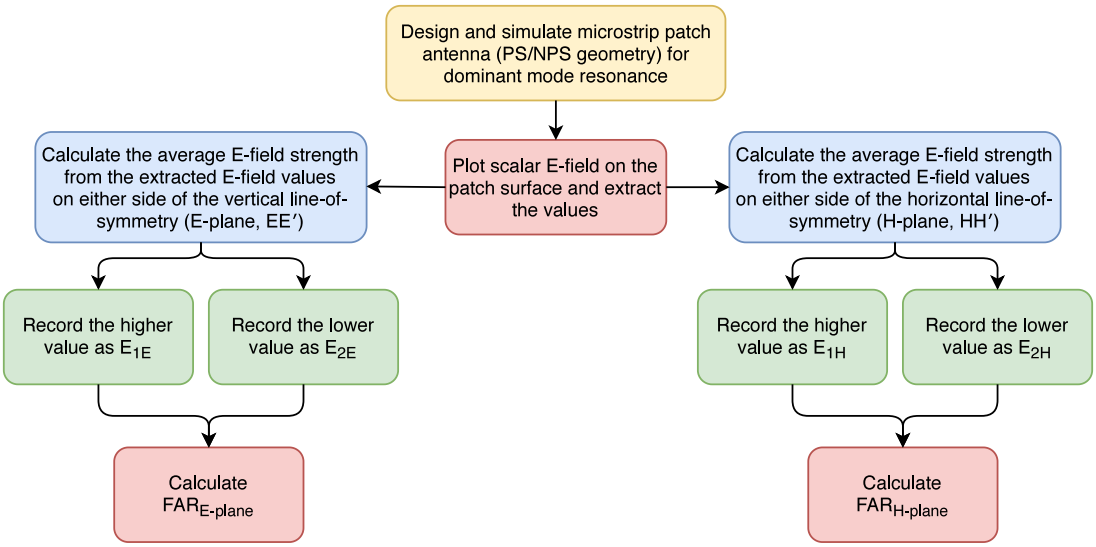

Fig. 3. Detailed flowchart enlisting the steps for calculating FAR for any patch geometry (PS/NPS).

Table 1
FARs and structural symmetry information for the conventional patch geometries under test.

Patch Geometry Classification	Microstrip Patch Geometry	No. of Sides (n)	Probe Position ρ (mm)	Impedance $\lvert Z\rvert$ (Ω)	$FAR_{E-plane}$	$FAR_{H-plane}$	BXPD in H-plane (dB)	Key factor for XP generation
Conventional NPS	TMSA	3	3.2	51.7	0.05	0.29	28	Structural Asymmetry + Probe Position Asymmetry
Conventional PS	SMSA	4	3.7	49.2	0.06	0.20	35	Probe Position Asymmetry

The above analysis indicates that the patch structures possessing inherent asymmetry in geometry (i.e. NPS-TMSA) suffer more from field asymmetry (i.e. higher FAR) and thus offer lower XPD in both the principal radiation planes compared to the PS geometry (SMSA).

In this context, it is important to note that for a patch of rectangular shape which is an irregular polygon having point symmetric geometry, XP varies with the change in aspect ratio without affecting the fundamental resonating mode. But, for the regular polygon like triangle, square, hexagon, circle, etc. any change in aspect ratio will make their shapes irregular which will enforce the electric field distributions and fundamental resonating modes change drastically. Hence, using this FAR parameter one can easily choose the suitable regular patch geometries capable of offering inherently high XPD (i.e. lower XP). Out of the two XP generating factors identified- *geometrical asymmetry* and *offset feed location*, it is viable to tackle the latter using a standard XP suppressing tool compared to the former.

Therefore, focusing on the need for achieving high BXPD for tracking and surveillance radar, only PS geometry (SMSA) is chosen for further enhancement of XPD using CCSP, a standard XP suppressing tool.

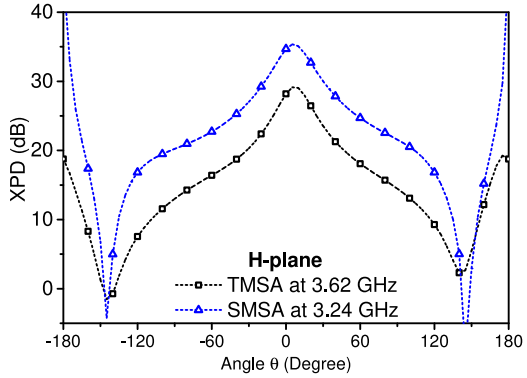

Fig. 4. XPD plot of the regular patch geometries under test in the H-plane.

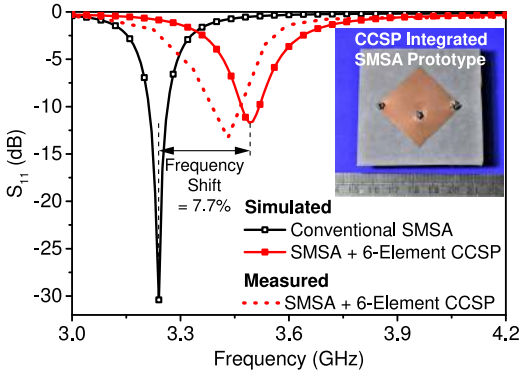

Fig. 6. S_{11} vs. frequency plot of SMSA with and without CCSP. Snapshot of the fabricated prototype is displayed in the inset.

3. Enhancement of XPD in point-symmetric patch geometries using CCSP

3.1. Point-symmetric antenna geometries and prototype

The detailed layout of the PS antenna geometry (SMSA) with CCSP is shown in Fig. 5. The antenna is designed for S-band applications using the same substrate as discussed in Section 2.2. Initially, a square patch operating at fundamental mode is designed with radius a_S = 18.36 mm and probe offset position ρ = 4.5 mm. The ground plane size is taken to be 4 times the patch radius (a_S). A pair of CCSP structures, each having radius of R = 3 mm, element diameter D = 0.5 mm and the number of elements n = 6 placed at an angular spacing of α = 60°, are loaded symmetrically at a peripheral location of r = 15.7 mm from the center along the patch radius.

3.2. Results and discussion

The simulated and measured S_{11} characteristics for SMSA are shown in Fig. 6. It is evident from the S_{11} characteristics that the incorporation of CCSP structures inside the PS square patch under consideration leads to a resonance frequency shift of 7.7% only.

The patch E-field distribution for SMSA with and without CCSP is investigated in Fig. 7 to assess the capability of CCSP structures in negating the field asymmetry resulting from offset probe feeding, the key contributor behind low XPD in PS geometry. The initial levels of asymmetry in E-field distribution observed on either side of the H-plane for conventional SMSA are found to be effectively counter-balanced after loading CCSP at the non-resonant vertices of the patch.

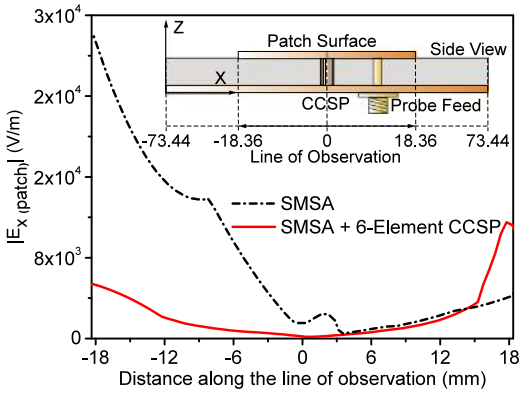

Fig. 7. E-field distribution plot of SMSA with and without CCSP observed on the patch surface along the x-axis. The line of observation is the line tracing the E-plane.

FAR values of the selected CCSP integrated SMSA along both the principal radiation planes are calculated from the dominant mode E-field distribution, as shown in Fig. 8 and are tabulated in Table 2. The $FAR_{E-plane}$ and $FAR_{H-plane}$ values for CCSP loaded SMSA are 0.019 and 0.134, respectively. A reduction in patch field asymmetry by 4% in E-plane and 7% in H-plane is obtained in CCSP loaded SMSA compared to the conventional SMSA. Thus, the significantly high patch field asymmetry across the H-plane in PS geometry can be easily reduced by loading CCSP structures on the patch along the H-plane.

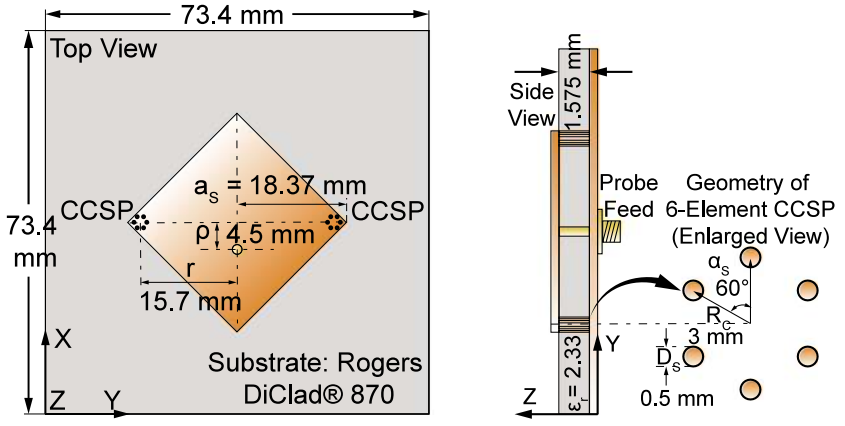

(a) Square Patch (b) Antenna side view and CCSP dimension

Fig. 5. Layout of CCSP integrated patch antenna having PS geometry (SMSA).

Table 2
FARs and XPD information for the square-shaped PS patch geometry.

Microstrip Patch Geometry	$FAR_{E-plane}$	$FAR_{H-plane}$	BXPD in H-plane (dB)
Conventional SMSA	0.06	0.20	35
SMSA + CCSP	0.019	0.134	62

Table 3
Performance comparison between the proposed work and some existing works on XP characterization and suppression.

Compared structure	PS/NPS patch geometry	Regular /Irregular patch geometry	XP analysis method	XP suppression tool	XPD at the boresight (dB)	XPD at $\theta = \pm 15°$	XPD at $\theta = \pm 30°$
Ref. [7]	PS (Circle)	Regular	Modal Analysis	Dot DGS	50	27	24
	PS (Circle)	Regular	Modal Analysis	Annular Ring DGS	45	27	22
	PS (Circle)	Regular	Modal Analysis	Arc DGS	40	29	31
Ref. [8]	PS (Square)	Regular	Modal Analysis	R-DGS	37	29	30
	PS (Circle)	Regular	Modal Analysis	R-DGS	40	29	32
	PS (Rectangle)	Irregular	Modal Analysis	R-DGS	33	29	31
Ref. [11]	PS (Square)	Regular	Surface Current Distribution	H-DGS	36	33	31
Ref. [12]	PS (Circle)	Regular	Modal Analysis	Pair of 6-element CCSP	50	36	35
Ref. [14]	PS (Circle)	Regular	Near-Field Analysis	Pair of ECSP	55	34	35
Ref. [15]	PS (Rectangular)	Irregular	Surface Current Distribution	Metasurface Layer	30	26	27
Ref. [16]	PS (Circle)	Regular	Feed Current Distribution	Capacitive Feed	30	26	23
Proposed	**PS (Square)**	**Regular**	**Field Asymmetry Ratio (FAR)**	**Pair of 6-element CCSP**	**45**	**35**	**35**

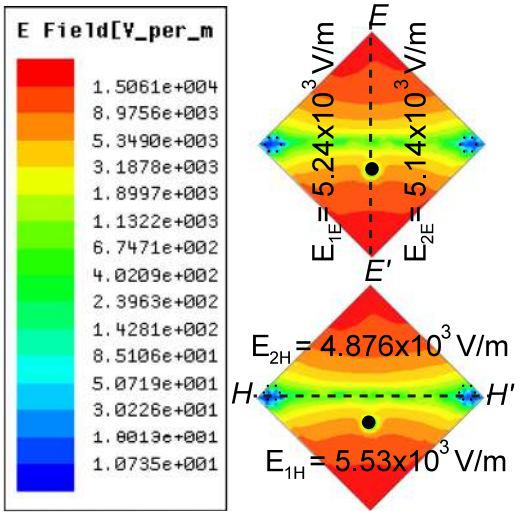

Fig. 8. Dominant mode E-field distribution for CCSP integrated SMSA. Black dot represents the feed location. All values indicated on the patch are the respective average E-field strengths in that region.

Simultaneously, the variation of simulated XPD values over the full range of azimuth (ϕ) and elevation (θ) angles with and without CCSP are studied for SMSA in detail through XPD contour plots as shown in Fig. 9. The XPD levels for conventional SMSA approximately range from 29 dB to 64 dB for all θ across both the principal radiation planes with 35 dB at the boresight. The XPD levels at the angular region of $\theta = \pm 30°$ on either side of boresight are found to be around 30 dB in the H-plane. The CCSP integrated square shaped PS patch geometry display comparatively higher XPD levels as depicted in Fig. 9.b. XPD levels as high as 34 dB to 62 dB is observed in H-plane. The BXPD level in the H-plane is increased by 27 dB. The XPD levels at the angular region of $\theta = \pm 30°$ on either side of boresight are found to be within 35 dB in the H-plane.

The far-field radiation characteristics of the CCSP integrated SMSA prototype are measured over both the E and H-plane respectively and are shown in Fig. 10. In the angular region of $\theta = \pm 30°$ the XPD levels for the antenna prototype under test are approximately in between 35 dB to 40 dB in H-plane. Significantly high XPD levels of greater than 40 dB is observed at the antenna boresight in both the principal radiation planes with approximately 35–40 dB in the angular region of $\theta = \pm 15°$ for H-plane. The process of incorporating multiple shorting pins during the fabrication of the prototype involves precise drilling of twelve holes inside the substrate and soldering. The entire process is done manually. Therefore, a minor deviation of the measurement results by 1.7% from the simulation has been observed. This difference between simulation and measurement results is primarily due to minor errors introduced during the fabrication process.

The CCSP integrated SMSA operates with a gain of 7.5 dBi. The effect of loading multiple shorting pins (a pair of 6-element CCSP) on the radiation efficiency of the conventional SMSA is also studied. The radiation efficiency vs. frequency characteristics of the conventional SMSA and SMSA with CCSP is shown in Fig. 11. It shows that the radiation efficiency of the antenna is not compromised due to loading of multiple shorting pins but a minor improvement in the radiation efficiency of SMSA is observed. The CCSP loaded SMSA radiates with 97% efficiency.

A performance comparison between the proposed work and some existing works based on the cross-polarization (XP) analysis method, patch geometry, XP suppression tool and XPD at different angular width (as per ETSI standard) is presented in Table 3. It is observed that the XP suppression studies presented till date are mostly based on modal analysis of the desired and higher order modes [7,8,12]. Few of the studies are based on the surface current distribution on the radiating patch/ground/feed [11,15,16]. Near-field distributions from the radiating patch have also been studied for XP analysis in [14]. In all these studies the direction of the E-field/current vectors needs to be observed minutely for better XP characterization. But the proposed FAR method is a magnitude based approach where only the magnitude of the E-field distribution on the radiating patch is taken into consideration. Therefore, the proposed method is simple for XP characterization of microstrip antenna patches of any shape (PS/NPS geometry).

Also, coincidentally in almost all of the research works documented so far on XP suppression, PS patch geometries have been used. However, the importance of point-symmetry in patch geometry was not

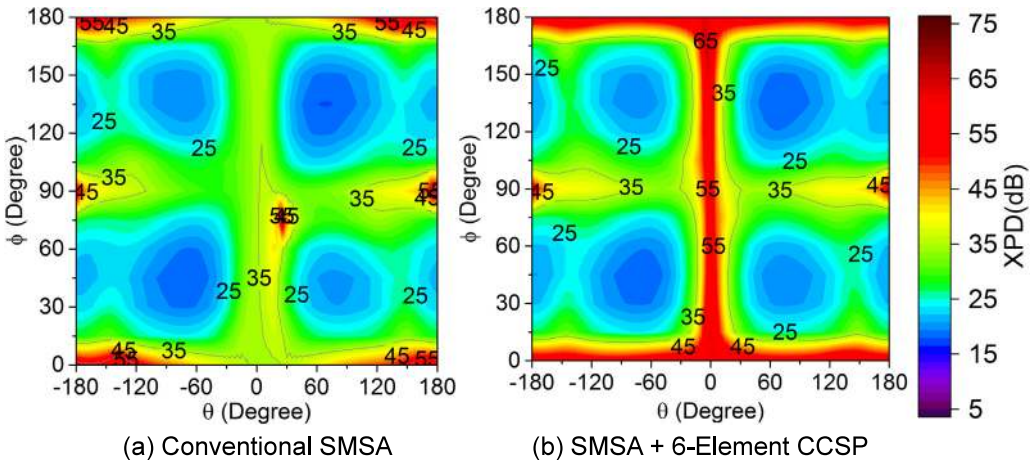

Fig. 9. XPD contour of square shaped PS patch geometry over the full range of azimuth (ϕ) and elevation (θ) angles.

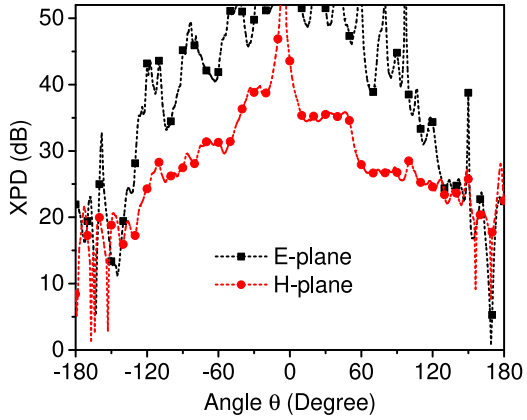

Fig. 10. Measured XPD patterns of CCSP integrated square shaped PS patch geometry.

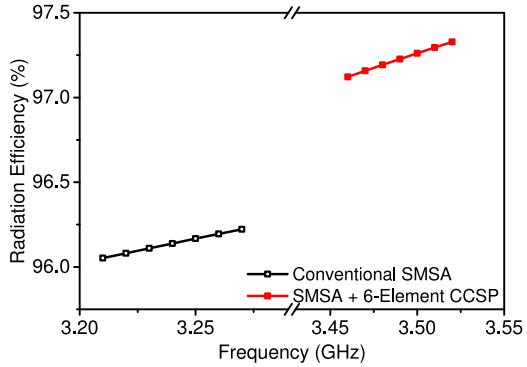

Fig. 11. Simulated radiation efficiency vs. frequency characteristic of conventional SMSA and CCSP integrated SMSA.

analyzed explicitly and the XP characterization of different non-point symmetric geometries has remained unattended. Therefore, the proposed FAR analysis method through the simple XP characterization of microstrip patch antennas of any shape (PS/NPS geometry) opens up new scopes to explain the XP performance of microstrip patch antennas having any arbitrary patch shape.

4. Conclusion

The correspondence of FAR and XPD for different types of commonly used patch geometries (TMSA and SMSA) has been validated in this paper. The novelty of this work is in characterizing the XP radiation for both PS and NPS patch geometries using a magnitude-based approach which is simpler than any other existing vector-based approaches like modal analysis, near field analysis, surface current analysis, etc. It can be certainly concluded that for high accuracy applications, only PS geometries should be chosen before applying any technique for XP suppression as NPS geometries exhibit high FAR values due to their inherent structural asymmetry leading to high XP radiation. Also, the proposed FAR analysis quantifies the level of field asymmetry in microstrip patch antennas caused due to two factors — structural asymmetry (for NPS geometries) and probe position asymmetry (for both PS & NPS geometries) that together result in a higher level of XP radiation. Therefore, in this paper, the analysis has been focused on probe-fed microstrip patch antennas only. However, there is a scope of extending the proposed FAR analysis on microstrip patch antennas with different types of feeding mechanisms like microstrip line feed, aperture feed, CPW feed, etc in future. Also, the proposed FAR parameter can be used as an efficient tool to explain the XP performance of microstrip patch antennas having any arbitrary patch shape.

Acknowledgments

The authors wish to thank Rogers Corporation for providing the substrate materials to fabricate the antenna prototypes.

Declaration of competing interest

The authors declare that they have no known competing financial interests or personal relationships that could have appeared to influence the work reported in this paper.

References

[1] Ghobrial SI. Cross-polarization in satellite and earth-station antennas. Proc IEEE 1977;65(3):378–87.
[2] Fixed Radio Systems. Characteristics and requirements for point-to-point equipment and antennas; part 4: antennas. 650 Route des Lucioles, F-06921 Sophia Antipolis Cedex, France: European Telecommunications Standards Institute (ETSI); 2017, https://www.etsi.org/deliver/etsi_en/302200_302299/30221704/02.01.01_60/en_30221704v020101p.pdf.
[3] Skolnik MI. Tracking radar. In: Radar handbook. 2nd ed.. New York, NY, USA: McGraw-Hill; 1990, p. 18.1–57 [ch. 18].
[4] Oberhart ML, Lo YT, Lee RQH. New simple feed network for an array module of four microstrip elements. Electron Lett 1987;23(9):436–7.
[5] Huynh T, Lee KF, Lee RQ. Cross polarisation characteristics of rectangular patch antennas. Electron Lett 1988;24(8):463–4.
[6] Lee KF, Luk KM, Tam PY. Crosspolarisation characteristics of circular patch antennas. Electron Lett 1992;28(6):587–9, 12.

[7] Kumar C, Guha D. Nature of cross-polarized radiations from probe-fed circular microstrip antennas and their suppression using different geometries of defected ground structure (DGS). IEEE Trans Antennas and Propagation 2012;60(1):92–101.
[8] Kumar C, Guha D. Reduction in cross-polarized radiation of microstrip patches using geometry-independent resonant-type defected ground structure (DGS). IEEE Trans Antennas and Propagation 2015;63(6):2767–72.
[9] Bhardwaj S, Rahmat-Samii Y. Revisiting the generation of cross polarization in rectangular patch antennas: A near-field approach. IEEE Antennas Propagat Mag 2014;56(1):14–38.
[10] Samanta S, Reddy PS, Mandal K. New dimension in cross-polarization reduction of a hexagonal microstrip antenna using two circular substrate integrated cavities. In: TENCON 2017-2017 IEEE region 10 conference. 2017, p. 1358–63.
[11] Acharjee J, Mandal K, Mandal SK. Reduction of mutual coupling and crosspolarization of a MIMO/Diversity antenna using a string of H-shaped DGS. AEU - Int J Electron Commun 2018;97.
[12] Samanta S, Reddy PS, Mandal K. Cross-polarization suppression in probe-fed circular patch antenna using two circular clusters of shorting pins. IEEE Trans Antennas and Propagation 2018;66(6):3177–82.
[13] Samanta S, Mandal K, Reddy PS, Sarkar PP. Investigation on novel quarter-arc shaped clusters of shorting pins for improvement in cross-polarization discrimination of diamond-shaped microstrip patch antenna. In: 2018 IEEE Indian conference on antennas and propagation. 2018, p. 1–4.
[14] Samanta S, Reddy PS, Mandal K, Sarkar PP. Near-field approach towards enhanced suppression of cross-polarised radiation across different elevation planes using novel epsilon-shaped clusters of shorting pins. IET Microw Antennas Propag 2019;13(7):966–75.
[15] Fartookzadeh M, Hossein S, Armaki M. Efficiency improvement and crosspolarization reduction of single-fed frequency-scan leaky wave microstrip antennas by using an M-shape metasurface as the WAIM layer. AEU - Int J Electron Commun 2019;116.
[16] Sarkar C, Guha D, Kumar C, Antar YMM. New insight and design strategy to optimize cross-polarized radiations of microstrip patch over full bandwidth by probe current control. IEEE Trans Antennas and Propagation 2018;66(8):3902–9.
[17] Kumar G, Ray KP. Broadband microstrip antennas. Norwood, MA: Artech House; 2003.
[18] Garg R, Bhartia P, Bahl II. Microstrip antenna design handbook. Norwood, MA, USA: Artech House; 2001.